

Article

Free-Standing $\text{Li}_4\text{Ti}_5\text{O}_{12}$ /Carbon Nanotube Electrodes for Flexible Lithium-Ion Batteries

Jun-Seok Lee ¹, Sang-Du Yun ², Oyunbayar Nyamaa ¹, Jeong-Hyeon Yang ² , Sun-Chul Huh ¹ ,
Hyo-Min Jeong ¹ , Tae-Hyun Nam ³, Yeon-Ju Ryu ³ and Jung-Pil Noh ^{1,*} 

- ¹ Department of Energy & Mechanical Engineering, Institute of Marine Industry, Gyeongsang National University, Tongyeonghaean-ro 2, Tongyeong 53064, Republic of Korea
² Department of Mechanical System Engineering, Gyeongsang National University, Tongyeonghaean-ro 2, Tongyeong 53064, Republic of Korea
³ Department of Materials Engineering and Convergence Technology, Gyeongsang National University, Jinju-daero 501, Jinju 52828, Republic of Korea
* Correspondence: nohjp@gnu.ac.kr

Abstract: Lithium-ion batteries (LIBs) have been used in many fields, such as consumer electronics and automotive and grid storage, and its applications continue to expand. Several studies have attempted to improve the performance of LIBs. In particular, the use of high-capacity silicon and tin as anodes has been widely studied. Although anodes composed of silicone and tin have high theoretical capacities, poor electrical conductivity and considerable volume expansion of such anodes deteriorate the LIB performance. Thus, $\text{Li}_4\text{Ti}_5\text{O}_{12}$ (LTO), a zero-strain material, has attracted much attention with high cycle stability and rate capability through improved electrical conductivity. However, LTO has the disadvantages of a low electrical conductivity (10^{-8} to 10^{-13} S cm^{-1}) and moderate Li^+ ion diffusion coefficient (10^{-9} to 10^{-16} $\text{cm}^2 \text{s}^{-1}$). In this study, the flexible and free-standing composite films were fabricated using only LTO and multi-walled carbon nanotube (CNT) with high electrical conductivity and ion diffusivity. The prepared LTO/CNT films showed a higher charge/discharge capacity than the theoretical capacity of the LTO electrode.

Keywords: LTO; buckypaper; Li-ion battery; flexible; free-standing



Citation: Lee, J.-S.; Yun, S.-D.; Nyamaa, O.; Yang, J.-H.; Huh, S.-C.; Jeong, H.-M.; Nam, T.-H.; Ryu, Y.-J.; Noh, J.-P. Free-Standing $\text{Li}_4\text{Ti}_5\text{O}_{12}$ /Carbon Nanotube Electrodes for Flexible Lithium-Ion Batteries. *Energies* **2022**, *15*, 8585. <https://doi.org/10.3390/en15228585>

Academic Editor: Mohammad (Mim) Rahimi

Received: 10 October 2022
Accepted: 7 November 2022
Published: 16 November 2022

Publisher's Note: MDPI stays neutral with regard to jurisdictional claims in published maps and institutional affiliations.



Copyright: © 2022 by the authors. Licensee MDPI, Basel, Switzerland. This article is an open access article distributed under the terms and conditions of the Creative Commons Attribution (CC BY) license (<https://creativecommons.org/licenses/by/4.0/>).

1. Introduction

Lithium-ion batteries (LIBs) are widely used in various fields, such as portable electronics and electric vehicles, owing to their high energy density and long cycle life [1]. However, the capacity loss increases due to additional reactions, such as solid electrolyte interphase (SEI) film formation and active material dissolution [2]. Much research is being conducted to develop new electrodes with improved stability and long cycle life at high current rates [3–8]. $\text{Li}_4\text{Ti}_5\text{O}_{12}$ (LTO), an anode material with a theoretical capacity of 175 mAhg^{-1} , possesses fast charge–discharge characteristics. Because LTO is a zero-strain material that does not change its structure during intercalation and deintercalation, a stable charge–discharge can be achieved even at high C-rate values. Therefore, lithium (Li) secondary batteries using LTOs as anodes have satisfactory and fast-charging properties. However, LTOs have the disadvantages of a low electrical conductivity (10^{-8} to 10^{-13} S cm^{-1}) and moderate Li^+ ion diffusion coefficient (10^{-9} to 10^{-16} $\text{cm}^2 \text{s}^{-1}$) [9,10]. Various methods, such as using nano-sized LTO particles, doping with other metal ions, surface modification using a metal or metal oxide, and coating with a conductive material, have been studied to improve electrical conductivity and ion diffusivity by reducing the ion diffusion path of Li^+ [11–15]. Among these methods, the carbon coating of LTO can improve the electrochemical performance of LTO by improving the surface electronic conductivity and electrical contact with the electrolyte [16–18]. Multi-walled carbon nanotubes (MWCNTs) have high electrical conductivity (approximately 10^3 – 10^5 S cm^{-1}), excellent mechanical properties,

and are lightweight [16,18]. It has been reported that there are the sol-gel method [19], blade method [20], and water-based process [21] for manufacturing electrodes. The sol-gel method can be synthesized at a low temperature close to room temperature and is inexpensive. However, it has the disadvantage of wrinkling or folding the edges, as it shrinks during drying. The blade method has advantages such as short working time, large-area production, and low-cost roll-to-roll production, but aggregate or crystallite formation at high concentration often occurs. The water-based process has a simpler manufacturing process compared to other electrode manufacturing methods and has the advantage of not being toxic because distilled water is used as a solvent.

Recently, we fabricated a flexible free-standing anode using buckypaper made from acid-treated MWCNT, and a silicon (Si) thin film was applied on the anode electrode [22]. It is known that buckypaper, instead of a copper (Cu) foil, can be used as a current collector and that the MWCNT matrix can improve the performance of a Si thin film. In this study, LTO was mixed with an acid-treated MWCNT with good electrical and ionic conductivity to compensate for the low electrical conductivity and moderate Li-ion diffusion coefficient.

2. Experiment

2.1. Materials and MWCNT

MWCNT was purchased from Carbon Nano-Material Technology Co. (Pohang, Republic of Korea) and LTO nanopowder from SAT Nano Technology Material Co. (Guangdong, China). The mixed cellulose ester (MCE)-based membrane filter used the model MCE04547A from Hyundai Micro Co. (Seoul, Republic of Korea). To convert the powder form of MWCNT into a paper-like form, we used an acid treatment to generate carboxyl. For the acid treatment method, MWCNT was added to a solution of HCl (35%) and distilled water in a ratio of 1:1 (vol.%) to a solution of HNO₃ (65%) and distilled water in a ratio of 1:2 (vol.%), and to a solution of HNO₃ (65%) and H₂SO₄ (98%) in a ratio of 1:3 (vol.%). Each of these MWCNT solutions was magnetically stirred at 60 °C for 3 h. In addition, the solution composed of MWCNT, HNO₃, and H₂SO₄ was sonicated at 60 °C for 3 h and cooled in ice water for 8 h. Subsequently, each MWCNT was neutralized with distilled water using a membrane filter and a vacuum pump until the pH became neutral. Further, each of them was dried in an oven at 60 °C for 24 h.

2.2. Fabrication of Electrodes

To compare the cycle performance of LTO anodes based on different amounts of CNT, three composite films with CNT:LTO in ratios of 60:40 wt.% (LC40), 50:50 wt.% (LC50), and 40:60 wt.% (LC60) were fabricated. The oxidized MWCNTs and LTO powders were dispersed in water, first by magnetic stirring for 1 h, followed by an ultrasonic bath for 3 h. The solution was filtered through a microporous membrane filter (pore size 0.45 μm) using filtration units with a vacuum pump. The resulting product was dried in an oven at 60 °C for 24 h. Finally, the LC films were peeled off from the filtration membrane. The thickness of the fabricated LC40, LC50, and LC60 films were approximately 0.058, 0.059, and 0.062 mm, respectively. To validate the electrochemical role of CNT and LTO in a composite film, LTO was coated on a Cu foil to manufacture an electrode (LTO_Cu), while oxidized CNT was used to manufacture a buckypaper (BP) electrode. Figure 1a–c are digital photographs captured after bending the LC film electrodes; the images validate that the electrodes are flexible and are not structurally damaged when bent. Regardless of composition (CNT:LTO), the films exhibited flexible properties.

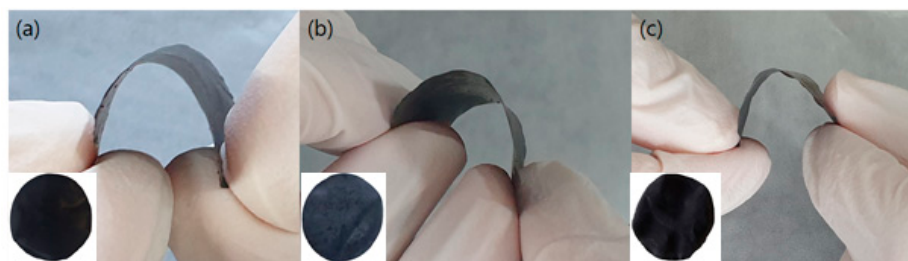


Figure 1. Images of the (a) LC40, (b) LC50, and (c) LC60 films.

2.3. Characterization Analyses

The LTO/CNT films were analyzed using X-ray diffraction (XRD, Ultima IV, Rigaku, Tokyo, Japan) with Cu K α radiation to determine the effect of any additional reactions that may occur in the process of mixing LTO and CNT on the structures. Morphological properties and particle size were observed using field emission scanning electron microscopy (FE-SEM, Mira3 LM, TESCAN, Brno, Czech Republic) at 15 kV. In a glove box filled with argon, Li foil and LTO_CNT were used as a counter electrode and working electrode, respectively; a 1 M solution of LiPF₆ was used in ethylene carbonate; diethyl carbonate (1:1, vol.%) and microporous polypropylene membrane were used as an electrolyte and a separator for a CR 2032-type coin cell, respectively. A galvanostatic charge–discharge (CC) test was performed with a battery cycler (Won A-tech, WDSC3000s) at 1–3 V and 0.5 C in the sections in which CNT did not react and LTO did. Cyclic voltammetry (CV) was performed with a Gamry Instrument over a voltage range of 1–3 V and a scan rate of 0.01 mVs^{−1}. Electrochemical impedance spectroscopy (EIS, ZIVE SP2, ZIVE LAB, Seoul, Korea) was performed at 3 V from 0.1 Hz to 10 MHz.

3. Results and Discussion

XRD elucidates the crystal structure of particles contained in a film. XRD was performed to confirm that there were no chemical changes in the aqueous process of mixing LTO and CNT used to fabricate LTO/CNT films. XRD patterns of the CNT, LTO, and LC films are shown in Figure 2. In the XRD pattern of LTO, sharp diffraction peaks are observed at $2\theta = 18.5^\circ, 35.7^\circ, 43.4^\circ, 47.5^\circ, 57.3^\circ, 62.9^\circ, 66.2^\circ, 74.5^\circ, 75.5^\circ, 79.5^\circ,$ and 82.4° , corresponding to the (111), (311), (400), (331), (333), (440), (531), (533), (622), (444), and (551) planes, respectively. All diffraction peaks of the LTO powder could be indexed as a cubic spinel structure with the space group Fd $\bar{3}$ m, which agreed well with those in the Joint Committee on Powder Diffraction Standards (JCPDS) card No. 26-1198. No characteristic peaks are observed for other impurities, such as rutile and anatase TiO₂. In the XRD pattern of CNT powder, broad diffraction peaks are observed at $2\theta = 26^\circ$, corresponding to the (002) plane. Unlike the peaks observed in the XRD patterns of CNT, LTO, and LC films, those of powders are the same, even after mixing, and no different peaks appeared. This confirms that no chemical changes occur while mixing LTO and CNT during the preparation of the LC films. Although the ratio of CNT in each mixture is different, there are no significant differences. The results of the compositions did not change either, confirming that a water-based process can be successfully used to manufacture a free-standing LTO_CNT anode. Figure 3a,b show SEM images of the oxidized CNT and LTO powders, respectively. MWCNT has a thread-type structure, while LTO exhibits a white grain-type structure. The outer diameter of CNT is approximately 20 nm, and the size of LTO is less than 2 μ m. The surface image of LTO shows that the particles are angled, indicating that they are crystalline. Figure 3c–e show SEM images of the LC40, LC50, and LC60 films, respectively. The surface images of the LC films show that white particles of LTO are contained between the CNT network. LTO and CNT are fabricated using a water-based process, confirming that they are well-mixed. The LTO is wrapped in the CNT network, which exhibits good electrical conductivity and Li⁺ diffusivity [21]. Therefore, the electrical conductivity and Li⁺ diffusivity of the electrodes are expected to improve.

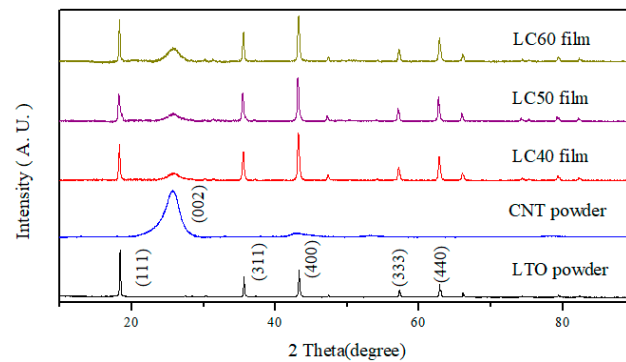


Figure 2. X-ray diffraction patterns of buckypaper, LTO, and the LC films.

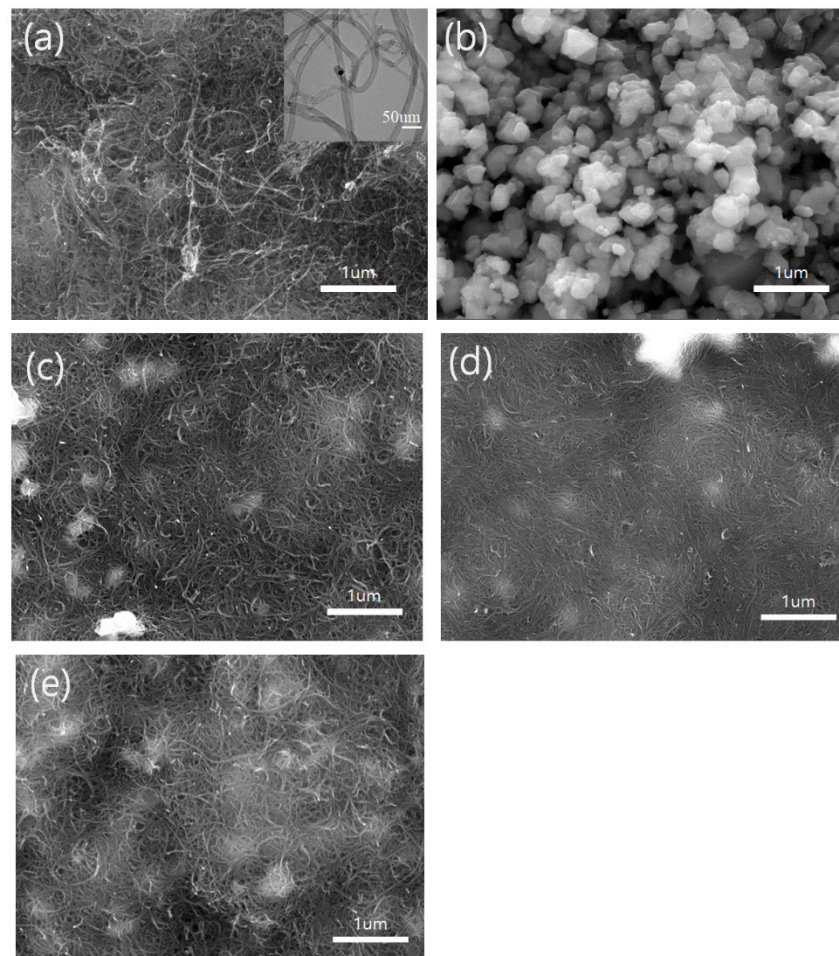


Figure 3. Field emission scanning electron microscopy surface images of (a) oxidized CNT powder and TEM image (inset), (b) LTO nanopowder, (c) LC40 film, (d) LC50 film, and (e) LC60 film.

To determine the response voltage of the LC film, we performed a periodic voltammogram (CV) test. Figure 4a–c show the resulting CV graph of the LC40, LC50, and LC60 films at a scan rate of 0.1 mVs^{-1} and a voltage range of 1–3 V. All ratios of CNT:LTO in the LC films have irreversible reaction capacities at 1.62 V in the discharge part of the first cycle. This was the result of creating a solid electrolyte interface. Two pairs of reversible redox peaks can be clearly seen for all ratios of CNT:LTO in the LC films. A pair of cathodic/anodic peaks can be clearly seen at 1.33 V/1.73 V for all the LC films in the first cycle; this can be attributed to the reduction of $\text{Li}_4\text{Ti}_5\text{O}_{12}$ to $\text{Li}_7\text{Ti}_5\text{O}_{12}$.



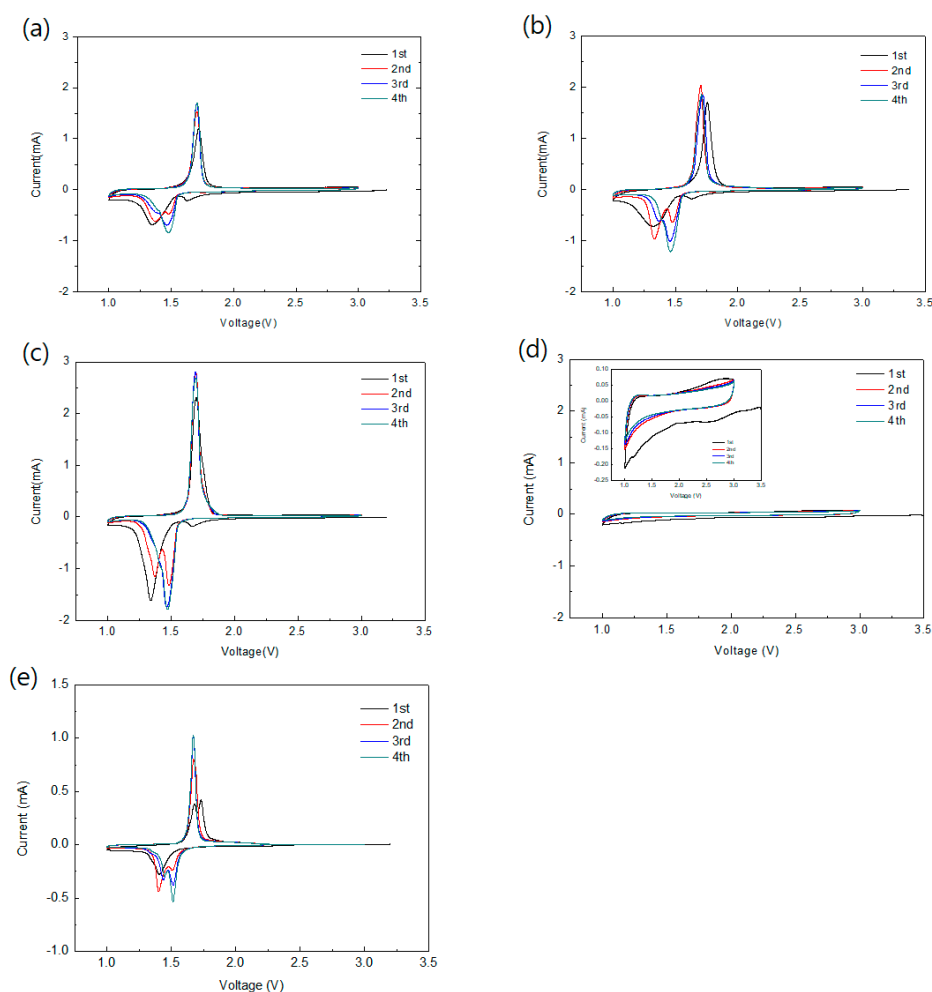


Figure 4. Cyclic voltammetry results for the (a) LC40 film, (b) LC50 film, (c) LC60 film (d) buckypaper, and (e) LTO_Cu electrode in the first through fourth cycles at 0.1 mV/s in a voltage window of 1–3 V (vs. Li⁺/Li).

Li⁺ paths were established and stabilized during the intercalation/deintercalation of Li⁺. Therefore, the cathodic/anodic peaks for all the LC films move from 1.33 V to 1.47 V and from 1.73 V to 1.70 V. The area of the LC films confirms that a higher amount of LTO leads to the formation of larger areas of the LC films. Because LTO only responds to a voltage range of 1–3 V vs. Li/Li⁺, the anode capacity increases with the amount of LTO. Figure 4d shows the CV graph of the fabricated BP. No peaks are observed at 1–3 V, reflecting the fact that CNT does not chemically react with Li⁺ at 1–3 V. However, a small area that indicates the film capacity can be seen and may be the result of Li⁺ intercalation/deintercalation in the porous structure. This verifies not only that the electrical conductivity and Li⁺ diffusion coefficient improves, but also that the capacity of the LC films increases. Figure 4e shows the CV graph of the LTO_Cu film. Cathodic/anodic peaks can be clearly seen at 1.4 V/1.73 V and 1.48 V in the first cycle. A cathodic/anodic peak of an LTO_Cu film moved from 1.4 V to 1.5 V and 1.73 V to 1.67 V during the cycle.

Figure 5a–e show charge/discharge graphs of the CC test with a current density of 1 C and a voltage range of 1–3 V vs. Li/Li⁺ to produce the LC40, LC50, and LC60 films, BP, and LTO_Cu film, respectively. The LC films show flat areas at 1.62 V and 1.33 V in the discharge section and 1.72 V in the charge section in the first cycle. As the cycles progressed, the flat area of the discharge and charge sections change to 1.47 V and 1.70 V, as shown in the CV test (Figure 4a–e). Comparing the capacity of the discharge and charge sections shows that the LC films have a high irreversible capacity in the cycle. The CC graphs representing BP (Figure 5d) and the LTO_Cu film (Figure 5e) indicate that the solid

electrolyte interface film of LTO is generated at 1.62 V, and Li ions are intercalated into the porous structure in the first cycle of BP and then could not deintercalate. Among these CC test results, the irreversible capacity of BP accounts for a large percentage. Therefore, a higher amount of CNT leads to a higher irreversible capacity of the material in the first cycle. However, the porous structure of CNT allows for an additional Li⁺ storage capacity. After the 100th cycle, the LC40, LC50, and LC60 films exhibit discharge capacities of 205.6 mAhg⁻¹, 192.0 mAhg⁻¹, and 192.6 mAhg⁻¹, respectively. These values are higher than that of recently published free-standing LTO electrode [23]. This is thought to be due to the porous structure. The porous structure of BP could be intercalated/deintercalated with Li⁺, and it has an additional capacity. Figure 6 shows that the cycle performance and coulombic efficiency (CE) as a percentage of the discharge capacity versus charge capacity of the LC films, BP, and the LTO_Cu cells, with a current density of 1 C and a voltage range of 1–3 V vs. Li/Li⁺. The capacities of all the LC films are higher than that of the LTO_Cu film (Figure 6e) because the porous structure of the CNT network-stored Li⁺. The cycle performance of BP (Figure 6d) exhibits a capacity of approximately 22 mAhg⁻¹ at 1–3 V after 20th cycle when Li⁺ intercalation/deintercalation is stabilized. BPs exhibit an irreversible capacity and poor CE (approximately 32–96%) from cycles 1 to 20. Li⁺ is intercalated in BP and cannot deintercalate from the porous structure of BP. Therefore, a higher wt.% of CNT leads to a lower CE value in the initial 20th cycle. All the LC films maintain a high CE value of more than 99% after 10th cycle and exhibit a low capacity reduction up to the 100th cycle. LC films could stabilize faster than BP because of the small amount of CNT. On comparing the capacity retention rates from the 10th cycle to the 100th cycle after cell stabilization, CE values of the LC40, LC50, and LC60 are verified as 98%, 96%, and 94.7%, respectively. A higher amount of CNT leads to an increased capacity retention rate, resulting in an improved electrode performance with good electrical conductivity and Li⁺ diffusivity of CNT. To further understand the improved conductivity in terms of carbon content, we performed EIS measurements before (Figure 7a) and after the 20th cycle (Figure 7b) for the LC film and LTO_Cu electrodes. EIS measurements were conducted in the frequency range of 0.1 Hz–1 MHz at 3 V. The intercept impedance on the real Z-axis represents the solution resistance, while the semicircle in the high–mid frequency range and the oblique line at low frequencies represent the charge-transfer process and the Li-ion diffusion process, respectively. The first resistance at the high frequency corresponds to the migration of Li ions across the passivation film (R_s), and the semicircle at the intermediate frequency corresponds to the charge-transfer reaction (R_{ct}). The R_s and R_{ct} values before and after the cycles of LC films and LTO_Cu are shown in Table 1. The R_s values of LC40 (4.81 Ω), LC50 (5.2 Ω), LC60 (4.64 Ω), and LTO_Cu (3.52 Ω) before the cycle demonstrate that the LC films have similar R_s values, and the LTO_Cu film has a lower R_s value than the LC films. After the cycle, the R_s values of LC40, LC50, LC60, and LTO_Cu are 5.91 Ω , 6.18 Ω , 5.82 Ω , and 3.42 Ω , respectively. The resistance value of the LC films increase by a small amount, and that of the Cu film hardly changes. The R_{ct} values of LC40, LC50, LC60, and LTO_Cu are 90.55 Ω , 98.88 Ω , 107.78 Ω , and 169.7 Ω , respectively, before the cycle. The R_{ct} values of the LC films are lower than that of the LTO_Cu film. These values demonstrate that a higher amount of CNT leads to a lower R_{ct} value. After the cycle, the R_s values of LC40, LC50, LC60, and LTO_Cu are 21.74 Ω , 35.34 Ω , 62.15 Ω , and 130.2 Ω , respectively. All electrodes have lower R_{ct} values after the cycle compared with those before the cycle. The R_{ct} values of LC40, LC50, LC60, and LTO_Cu decrease by 76%, 64.3%, 63.4%, and 23.3%, respectively. These results indicate that the process of mixing LTO with CNT affects the Li⁺ diffusion process, reflecting the superior electrical conductivity that the CNT/LTO composite film exhibits. As the cycle progresses, the connection between CNT and LTO is stabilized and inhibits polarization. Therefore, a higher amount of CNT results in improved cycle characteristics.

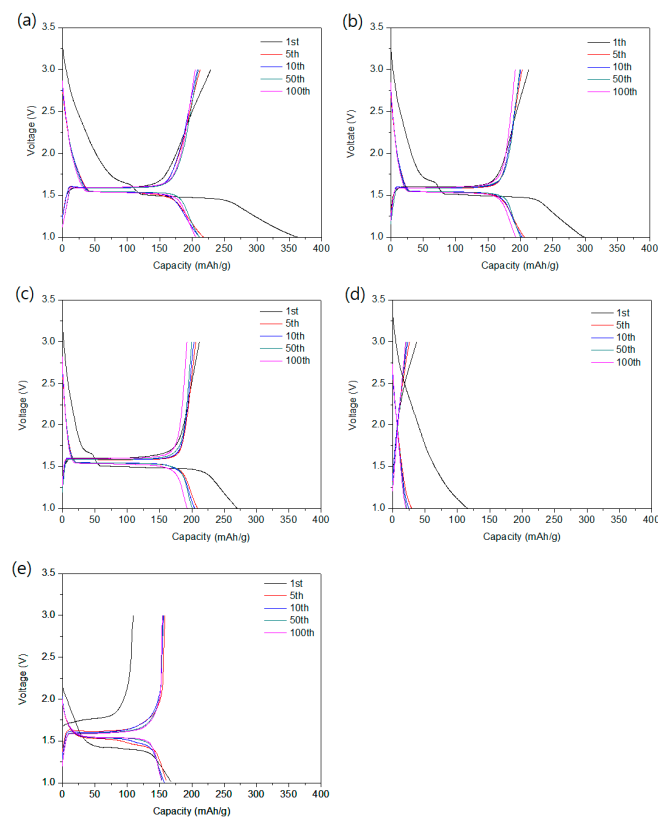


Figure 5. Discharge–charge curve of the (a) LC40 film, (b) LC50 film, (c) LC60 film, (d) buckypaper, and (e) LTO_Cu electrode at 1 C in the voltage window of 1–3 V (vs. Li^+/Li).

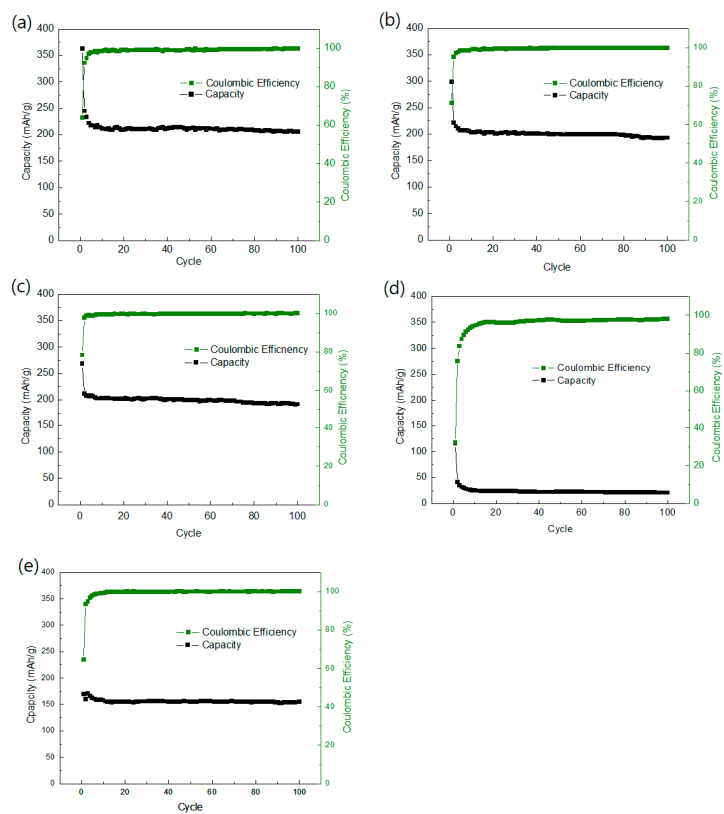


Figure 6. Capacity and coulombic efficiency curve of the (a) LC40 film, (b) LC50 film, (c) LC60 film, (d) buckypaper, and (e) LTO_Cu electrode at 1 C in the voltage window of 1–3 V (vs. Li^+/Li).

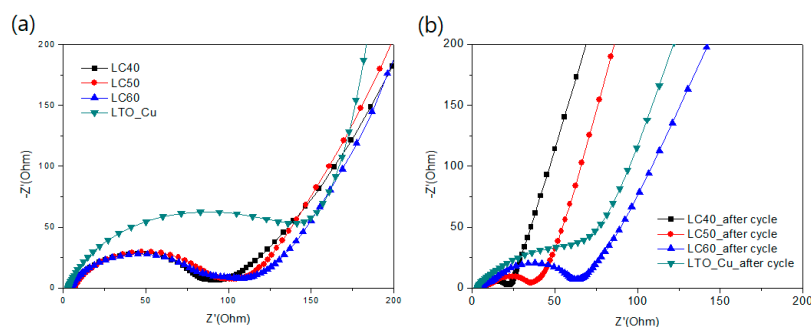


Figure 7. Nyquist impedance plots of the LC40, LC50, LC60 films, and LTO_Cu electrodes after (a) making cell and (b) 20th charge at 0.5 C, measured in the frequency range of 0.01 Hz–1 MHz (Z' : real part of impedance; Z'' : imaginary part of impedance).

Table 1. Physical properties and electrochemical impedance spectroscopy parameters of the LC films and LTO_Cu electrodes.

	LC40	LC50	LC60	LTO_Cu	LC40 after	LC50 after	LC60 after	LTO_Cu after
R_s (Ω)	4.81	5.2	4.64	3.52	5.91	6.18	5.82	3.42
R_{ct} (Ω)	90.55	98.88	107.78	169.7	21.74	35.34	62.15	130.2

4. Conclusions

In this study, flexible, binder-free, and free-standing electrodes were fabricated using acid-treated MWCNT. All three ratios of the films had flexible properties. Although they were manufactured using the water-based method, no chemical changes occurred in the materials, which were well-mixed. The CV test showed that LC films stabilized faster than the LTO_Cu films. The CC test demonstrated that a higher amount of CNT led to higher irreversible capacity in the first cycle; however, the cycle performance and additional capacity were improved. The application of LTO to CNT networks increased the electrical conductivity and ion diffusivity. The EIS test confirmed that the R_{ct} value was lower at higher CNT ratios, especially with a larger gap in the course of the cycle. The fabrication of the composite film using CNT confirmed that the excellent electrical conductivity and ion diffusivity of CNT improved the performance of the electrodes.

Author Contributions: Conceptualization, J.-P.N.; Methodology, H.-M.J.; Validation, J.-S.L. and O.N.; Formal analysis, J.-H.Y.; Investigation, S.-D.Y.; Data curation, T.-H.N., Y.-J.R. and J.-P.N.; Writing—original draft, J.-S.L.; Writing—review & editing, J.-S.L. and J.-P.N.; Project administration, S.-C.H. All authors have read and agreed to the published version of the manuscript.

Funding: This research was funded by the National Research Foundation of Korea (NRF) grant funded by the Korean Government (MSIT) (No. 2022R1A2C1008125) and the Korea Institute for Advancement of Technology (KIAT) grant funded by the Korean Government (MOTIE) (P0012748, The Competency Development Program for Industry Specialist).

Conflicts of Interest: The authors declare no conflict of interest.

References

- Qi, W.; Shapter, J.G.; Wu, Q.; Yin, T.; Gao, G.; Cui, D. Nanostructured anode materials for lithium-ion batteries: Principle, recent progress and future perspectives. *J. Mater. Chem. A* **2017**, *5*, 19521–19540. [[CrossRef](#)]
- Arora, P.; White, R.E.; Doyle, M. Capacity Fade Mechanisms and Side Reactions in Lithium-Ion Batteries. *J. Electrochem. Soc.* **1998**, *145*, 3647–3667. [[CrossRef](#)]
- Li, S.; Mao, J. Enhanced the electrochemical performance of Li₄Ti₅O₁₂ anode materials by high conductive graphene nanosheets. *J. Mater. Sci. Mater. Electron.* **2017**, *28*, 15135–15141. [[CrossRef](#)]
- Liu, Y.; Yan, X.; Xu, B.; Lan, J.; Yu, Y.; Yang, X.; Lin, Y.; Nan, C. Li₄Ti₅O₁₂ nanosheets assembled in tubular architecture for lithium storage. *Chem. Eng. J.* **2019**, *361*, 1371–1380. [[CrossRef](#)]

5. Xu, G.; Han, P.; Dong, S.; Liu, H.; Cui, G.; Chen, L. Li₄Ti₅O₁₂-based energy conversion and storage systems: Status and prospects. *Coord. Chem. Rev.* **2017**, *343*, 139–184. [[CrossRef](#)]
6. Khan, F.; Oh, M.; Kim, J.H. N-functionalized graphene quantum dots: Charge transporting layer for high-rate and durable Li₄Ti₅O₁₂-based Li-ion battery. *Chem. Eng. J.* **2019**, *369*, 1024–1033. [[CrossRef](#)]
7. Kang, J.; Dong, G.; Li, Z.; Li, L. Preparation and electrochemical properties of nanorods and nanosheets structural Li₄Ti₅O₁₂ as anode for lithium ion batteries. *J. Mater. Sci. Mater. Electron.* **2018**, *29*, 12615–12623. [[CrossRef](#)]
8. Lee, B.-G.; Ahn, H.-J.; Yoon, J.-R. Effects of post-calcination and mechanical pulverization on the electrochemical properties of nano-sized Li₄Ti₅O₁₂ for hybrid capacitors. *Curr. Appl. Phys.* **2017**, *17*, 121–125. [[CrossRef](#)]
9. Zhao, B.; Ran, R.; Liu, M.; Shao, Z. A comprehensive review of Li₄Ti₅O₁₂-based electrodes for lithium-ion batteries: The latest advancements and future perspectives. *Mater. Sci. Eng. R. Rep. Rev. J.* **2015**, *98*, 1–71. [[CrossRef](#)]
10. Nitta, N.; Wu, F.; Lee, J.T.; Yushin, G. Li-ion battery materials: Present and future. *Mater. Today* **2015**, *18*, 252–264. [[CrossRef](#)]
11. Hou, L.; Qin, X.; Gao, X.; Guo, T.; Li, X.; Li, J. Zr-doped Li₄Ti₅O₁₂ anode materials with high specific capacity for lithium-ion batteries. *J. Alloys Compd.* **2019**, *774*, 38–45. [[CrossRef](#)]
12. Reza, C.; Hernowo, M.F.; Syahrial, A.Z.; Subhan, A.; Priyono, B. Improved Li₄Ti₅O₁₂ performance with addition of graphite and Sn nanoparticles using the solid-state method as half-cell lithium-ion battery anode. *AIP Conf. Proc.* **2020**, *2232*, 030004. [[CrossRef](#)]
13. Knabe, N.M.; Mhlongo, W.T.; McCrindle, R.I.; Zheng, H. The electrochemical effect of Al-doping on Li₄Ti₅O₁₂ as anode material for lithium-ion batteries. *Mater. Today Proc.* **2018**, *5*, 10592–10601. [[CrossRef](#)]
14. Lu, H.; Hagberg, J.; Lindbergh, G.; Cornell, A. Li₄Ti₅O₁₂ flexible, lightweight electrodes based on cellulose nanofibrils as binder and carbon fibers as current collectors for Li-ion batteries. *Nano Energy* **2017**, *39*, 140–150. [[CrossRef](#)]
15. Cho, H.; Son, H.; Kim, D.; Lee, M.; Boateng, S.; Han, H.S.; Kim, K.M.; Kim, S.; Choi, H.; Song, T.; et al. Impact of Mg-Doping Site Control in the Performance of Li₄Ti₅O₁₂ Li-Ion Battery Anode: First-Principles Predictions and Experimental Verifications. *J. Phys. Chem. C* **2017**, *121*, 14994–15001. [[CrossRef](#)]
16. Ye, Z.; Zhong, F.; Chen, Y.; Zou, Z.; Jiang, C. Unique CNTs-chained Li₄Ti₅O₁₂ nanoparticles as excellent high rate anode materials for Li-ion capacitors. *Ceram. Int.* **2022**, *48*, 20237–20244. [[CrossRef](#)]
17. Jiang, C.; Liu, S.; Lian, Q.; Zhao, J.; Ding, W.; Yu, Z.; Huang, R.; Zou, Z. Nitrogen-doped carbon-coated hierarchical Li₄Ti₅O₁₂-TiO₂ hybrid microspheres as excellent high rate anode of Li-ion battery. *Ceram. Int.* **2017**, *43*, 11354–11360. [[CrossRef](#)]
18. Kuo, Y.-C.; Lin, J.-Y. One-pot sol-gel synthesis of Li₄Ti₅O₁₂/C anode materials for high-performance Li-ion batteries. *Electrochim. Acta* **2014**, *142*, 43–50. [[CrossRef](#)]
19. Dehghanhadikolaei, A.; Ansary, J.; Ghoreishi, R. Sol-gel process applications: A mini-review. *Proc. Nat. Res. Soc.* **2018**, *2*, 02008. [[CrossRef](#)]
20. Aziz, F.; Ismail, A.F. Spray coating methods for polymer solar cells fabrication: A review. *Mater. Sci. Semicond. Process.* **2015**, *39*, 416–425. [[CrossRef](#)]
21. Piffet, C.; Vertruyen, B.; Caes, S.; Thomassin, J.-M.; Broze, G.; Malherbe, C.; Boschini, F.; Cloots, R.; Mahmoud, A. Aqueous processing of flexible, free-standing Li₄Ti₅O₁₂ electrodes for Li-ion batteries. *Chem. Eng. J.* **2020**, *397*, 125508. [[CrossRef](#)]
22. Nyamaa, O.; Seo, D.-H.; Lee, J.-S.; Jeong, H.-M.; Huh, S.-C.; Yang, J.-H.; Dolgor, E.; Noh, J.-P. High Electrochemical Performance Silicon Thin-Film Free-Standing Electrodes Based on Buckypaper for Flexible Lithium-Ion Batteries. *Materials* **2021**, *14*, 2053. [[CrossRef](#)] [[PubMed](#)]
23. Chaturvedi, P.; Kanagaraj, A.B.; Al Nahyan, M.S.; Al Shibli, H.; Ashoor, A.A.; Fadaq, H.; Al Dahmani, S.; Choi, D.S. Electrical and electrochemical properties of carbon nanotube-based free standing LTO electrodes for current collector-free Li-ion batteries. *Curr. Appl. Phys.* **2019**, *19*, 1150–1155. [[CrossRef](#)]